Eur. Phys. J. C (2025) 85:669
https://doi.org/10.1140/epjc/s10052-025-14399-0

THE EUROPEAN PHYSICAL JOURNAL C

Regular Article - Theoretical Physics

Nonlocal correlation in quantum network near a Schwarzschild black hole

Jia Ji[1,2], **Kan He**[1,a], **Shu-Yuan Yang**[1,b]

[1] Department of Mathematics, Taiyuan University of Technology, Taiyuan 030024, People's Republic of China
[2] College of General Education, Shanxi College of Technology, Shuozhou 036000, People's Republic of China

Received: 24 March 2025 / Accepted: 2 June 2025

Abstract We transfer the scenario of quantum network nonlocal correlation to the vicinity of a black hole's event horizon, aiming to evaluate the impact of Hawking effect on network nonlocality within this specific context. In an entanglement swapping network with two bipartite resources and three parties, we examine two scenarios with distinct Hawking radiation locations: one where it affects the endpoint parties' system and another where it impacts all parties' system. In both cases, network nonlocality decays due to Hawking radiation and disappears entirely when the Hawking temperature reaches a critical threshold. However, we observe a striking phenomenon: when resource states are maximally entangled and the affected system belongs to the endpoint participants, network nonlocality diminishes but does not vanish throughout the radiation process. Subsequently, we extend our investigation to star and chain networks to evaluate how resource quantity and distribution influence network nonlocality under Hawking radiation. Our results indicate that star networks exhibit greater resilience against Hawking radiation in maintaining nonlocality.

1 Introduction

Quantum technology is a key enabler for future communication infrastructure. Building on this potential, it can be used to construct relevant network architectures to promote space exploration [1]. Quantum technologies in space are explored and investigated [2], such as quantum key distribution for secure satellite communications [3], quantum-enhanced navigation systems [4], and quantum sensor networks [5] for earth observation.

In fact, quantum states emitted into space may have their correlations altered by environmental factors such as extreme temperatures, magnetic fields, and cosmic radiation [1]. This is because Einstein's theories predicted that the gravitational collapse of a massive enough star would form a black hole [6,7]. Furthermore, Stephen Hawking proposed that black holes emit radiation through quantum effects, a phenomenon now known as Hawking radiation [8]. Hawking radiation theory suggests that near a black hole's event horizon, quantum fluctuations can cause virtual particle pairs to separate, with some particles escaping as radiation while introducing thermal noise. This process serves as a crucial link between quantum mechanics and gravity, playing a central role in the infamous information paradox of black holes [9,10].

In recent years, many scholars have focused on investigating the changes that quantum resources undergo in curved spacetime, providing a crucial perspective and significant insights into the fundamental interactions between quantum mechanics and gravity. Among these studies, the impact of Hawking radiation on quantum resources in Schwarzschild spacetime has attracted particular attention. Research has covered topics including quantum steering [11,12], coherence [13], entanglement [14,15], discord [16], nonlocality [17–22], the entropy uncertainty relation [23], and quantum teleportation [24], yielding groundbreaking results. For example, Wu et al. [24] found that under a specific initial state, the Hawking effect can create net fidelity of quantum teleportation, offering new possibilities for the transmission of quantum information under extreme conditions. As research advances, some scholars have expanded their research focus to broader curved spacetime backgrounds [25,26] and other gravitational effects [27,28], further probing quantum resource behavior in complex environments. These studies provide new theoretical foundations for quantum mechanics and general relativity interactions and lay

[a] e-mail: hekan@tyut.edu.cn (corresponding author)
[b] e-mail: yangshuyuan2000@163.com (corresponding author)

Published online: 18 June 2025

groundwork for extreme-condition quantum information applications. However, it is worth noting that these studies are generally based on single source.

As the demand for large-scale, long-distance communication grows, many scholars are studying quantum correlations in quantum networks [29]. For example, researchers have explored the definition and criteria of nonlocal correlations in networks with different structures [30–32]. They have found that even if the resources are in mixed states, just one entangled state may lead to nonlocal correlations in the network. The network nonlocality, as an important quantum resource, fundamentally underlie various applications of quantum networks such as computing, sensing, and secured long-distance communications [33–36].

The generation of quantum correlations in a quantum network depends on its resources and topology. If a quantum network's topology is fixed, the multiple particles in the network may fall into the curved spacetime near a black hole. This differs from the evolution of single-source quantum entanglement under Hawking radiation. This may hinder the formation of quantum network nonlocal correlations in space and impact relevant application scenarios. It is natural to ask whether the network nonlocal correlations still exist under Hawking radiation. Since quantum networks with different structures show diverse characteristics under Hawking radiation, we can use this effect to explore more stable network structures. This question relates to quantum communication foundations and may inspire future space exploration communication technologies.

In this study, we first focus on the influence of Hawking radiation on nonlocal correlations in an entanglement swapping (ES) network in the context of the Schwarzschild black hole. Initially, we assumed that only the marginal parties fall freely toward the event horizon and then extended the setting to the entire network state. Secondly, we expanded the research to more general chain networks and star networks. Through calculations and numerical analysis, we found that the decay of nonlocal correlations in the network depends not only on the network's topology but also on the parameters and locations of the resource states within it. The structure of this article is as follows: in Sect. 2, we present the basic background knowledge required for the study; in Sect. 3, we give the general evolution law of states in curved spacetime; in Sect. 4, we present the main research results of this article; finally, in Sect. 5, we summarize the article.

2 Prerequisites

In this section, we briefly recall the quantization of Dirac fields in the background of Schwarzschild black hole and the network nonlocal correlations.

2.1 Dirac fields in the Schwarzschild space-time

In the present analysis, we choose the initial state to be of the fermionic type. This allows us to be on the same footing with other recent studies on quantum correlations in the relativistic setting, which frequently consider Dirac particles [14,24]. In our further discussion, for simplicity, the gravitational constant G, the Planck constant $\hbar$, the speed of light c, and the Boltzmann constant k_B are assumed to be equal to 1.

In order to describe the vacuum state of the curved spacetime for fermions, one can start with the following Dirac equation:

$$(i\gamma^a e_a^\mu D_\mu - m)\Phi = 0,$$

where m is the fermion mass, γ^a are the Dirac matrices, e_a^μ is vierbein, $D_\mu = \partial_\mu - \frac{i}{4} w_\mu^{ab}\sigma_{ab}$, $\sigma_{ab} = \frac{i}{2}\{\gamma_a, \gamma_b\}$, w_μ^{ab} is the spin connection, and Φ represents a spinor field.

By using the metric of the Schwarzschild black hole

$$ds^2 = -\left(1 - \frac{2M}{r}\right)dt^2 + \left(1 - \frac{2M}{r}\right)^{-1} dr^2 + r^2(d\theta^2 + \sin^2\theta d\varphi^2),$$

where r and M represent the radius and mass of the black hole, the solutions of the Dirac equation in regions I (the Universe, physically accessible) and II (inside the black hole, physically inaccessible) are given by [37]:

$$\Phi_{\mathrm{k}}^{I+} = \xi e^{-iwu}, \qquad \Phi_{\mathrm{k}}^{II+} = \xi e^{iwu}, \tag{1}$$

where k is the wave vector used to label the modes, ξ denotes the four-component Dirac spinor composed of the spinorial spherical harmonics, w is the monochromatic frequency of the Dirac field, $u = t - r_*$ with the tortoise coordinate $r_* = r + 2M\ln\frac{r-2M}{2M}$.

In order to obtain a complete basis for the analytic modes with positive energy, the Kruskal coordinates are utilized to perform analytical continuation in accordance with the Damour–Ruffini method [38]. The resulting Dirac fields are expanded in the appropriate Kruskal basis, as follows:

$$\Phi = \int d\mathrm{k} \frac{1}{\sqrt{2\cosh(4\pi M w)}} \times [c_{\mathrm{k}}^I \Phi_{\mathrm{k}}^{I+} + c_{\mathrm{k}}^{II}\Phi_{\mathrm{k}}^{II+} + d_{\mathrm{k}}^{I\dagger}\Phi_{\mathrm{k}}^{I-} + d_{\mathrm{k}}^{II\dagger}\Phi_{\mathrm{k}}^{II-}], \tag{2}$$

where $c_{\mathrm{k}}^{\mathbf{I}}$ and $d_{\mathrm{k}}^{\mathbf{I}^\dagger}$ with $\mathbf{I} = (I, II)$ are the fermion annihilation operators and antifermion creation operators acting on the Kruskal vacuum. The superscripts on the kets $\{+, -\}$ denote the particle and antiparticle vacua, respectively.

Next, by using the Bogoliubov transformation, it is possible to establish the relation between operators in a black hole and the Kruskal space-time [39]. In particular, the vacuum

and excited states of the black hole coordinates correspond to the Kruskal two-mode squeezed states as follows:

$$\begin{aligned} |0\rangle_{\mathrm{k}}^{+} &\rightarrow \lambda_{-}|0_{\mathrm{k}}\rangle_{I}^{+}|0_{-\mathrm{k}}\rangle_{II}^{-}+\lambda_{+}|1_{\mathrm{k}}\rangle_{I}^{+}|1_{-\mathrm{k}}\rangle_{II}^{-}, \\ |1\rangle_{\mathrm{k}}^{+} &\rightarrow |1_{\mathrm{k}}\rangle_{I}^{+}|0_{-\mathrm{k}}\rangle_{II}^{-}, \end{aligned} \tag{3}$$

with the Bogoliubov coefficients $\lambda_{\pm}=(e^{\pm\frac{w}{T}}+1)^{-\frac{1}{2}}$, where $T=\frac{1}{8\pi M}$ is the Hawking temperature [40]. Hereafter, for simplicity, we consider $\omega=1$, $|n_{\mathrm{k}}\rangle_{I}^{+}=|n\rangle_{I}$ and $|n_{-\mathrm{k}}\rangle_{II}^{-}=|n\rangle_{II}$.

2.2 Network nonlocal correlations

Considering a general network $\Xi_{q,n}$ consisting of q parties, namely, $\mathcal{A}_1, \mathcal{A}_2, \ldots, \mathcal{A}_q$, and n sources $\rho_1, \rho_2, \ldots, \rho_n$, each party $\mathcal{A}_i$ can perform the measurement labeled by $x_i (x_i \in \{0,1\})$ with its outcomes $a_i (a_i \in \{0,1\})$. The behavior of this network is local if its probability distribution satisfies

$$P(\mathbf{a}|\mathbf{x})=\int_{\Omega}\prod_{i=1}^{n}d\mu_i(\lambda_i)\prod_{j=1}^{q}p(a_j|x_j,\Lambda_j), \tag{4}$$

where $\mathbf{a}=(a_1,\ldots,a_q)$, $\mathbf{x}=(x_1,\ldots,x_q)$, λ_i denotes the hidden variable distributed by source ρ_i, $\mu_i(\lambda_i)$ is the probability distribution for λ_i with $\int\mu_i(\lambda_i)d\lambda_i=1$, and Λ_j denotes the set of classical variables associated with party $\mathcal{A}_j$. Otherwise, the behavior is network nonlocal [30]. Recall that a network is k-independent network if there are k parties that do not share any source with each other, and we denote $\Gamma=\{i_1,i_2,\ldots,i_k\}$ as the set of indices of all independent nodes. The joint correlations derived from a network with classical variables satisfy the following inequality [30]:

$$\mathcal{B}=|I(q,k)|^{\frac{1}{k}}+|J(q,k)|^{\frac{1}{k}}\leq 1 \tag{5}$$

where the correlators $I(q,k)$ and $J(q,k)$ are defined as

$$I(q,k)=\frac{1}{2^k}\sum_{x_j,j\in\Gamma}\langle A_{x_1}A_{x_2}\cdots A_{x_q}\rangle,$$

$$J(q,k)=\frac{1}{2^k}\sum_{x_j,j\in\Gamma}(-1)^{\sum_{j\in\Gamma}x_j}\langle A_{x_1}A_{x_2}\cdots A_{x_q}\rangle,$$

herein A_{x_i} is the observable of the party $\mathcal{A}_i$ $(i=1,2\ldots q)$ and $\langle A_{x_1}A_{x_2}\cdots A_{x_q}\rangle=\sum_{\mathbf{a}}(-1)^{\sum_{j=1}^{q}a_j}P(\mathbf{a}|\mathbf{x})$ and $P(\mathbf{a}|\mathbf{x})$ are defined in Eq. (4). This is a set of n-local nonlinear correlation inequalities derived from the assumption of k-independent network. Any violation of Ineq. (5) by a physical system will be seen as a nonlocality witness for the present network.

The chain network with $n+1$ parties and n sources shown in Fig. 1 can be considered as a 2-independent network. According to Ref. [41], with respect to the generic quantum state $\rho_{A^1A^2}\otimes\rho_{A^2A^3}\otimes\cdots\otimes\rho_{A^nA^{n+1}}$, the maximal value of $\mathcal{B}$ in Eq. (5) is given by

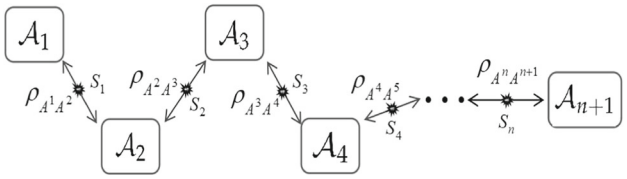

Fig. 1 The chain network scenario. Here, we choose $\mathcal{A}_1$ and $\mathcal{A}_{n+1}$ as the marginal node, and the source $\mathcal{S}_i$ distributes the quantum state $\rho_{A^iA^{i+1}}$ to party $\mathcal{A}_i$ and party $\mathcal{A}_{i+1}$ $(i=1,2\ldots n)$

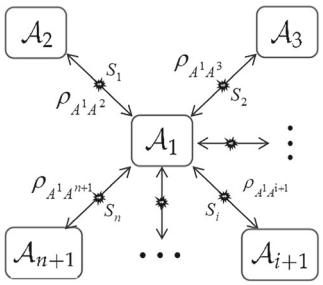

Fig. 2 The star network scenario. Here, we choose $\mathcal{A}_1$ as the intermediate node, and the source $\mathcal{S}_i$ distributes the quantum state $\rho_{A^1A^{i+1}}$ to party $\mathcal{A}_1$ and party $\mathcal{A}_{i+1}$ $(i=1,2\ldots n)$

$$\mathcal{B}_{\mathrm{chain}}^{\max}=\sqrt{\prod_{i=1}^{n}\delta_1^{(i)}+\prod_{i=1}^{n}\delta_2^{(i)}}, \tag{6}$$

where $\delta_1^{(i)}$ and $\delta_2^{(i)}$ are the two largest (positive) eigenvalues of the matrix $\sqrt{T^{\dagger}_{A^iA^{i+1}}T_{A^iA^{i+1}}}$ with $\delta_1^{(i)}>\delta_2^{(i)}$, and $T_{A^iA^{i+1}}$ is the correlation matrix of $\rho_{A^iA^{i+1}}$. Notably, in the subsequent discussion of this paper, the correlation matrix of the quantum state ρ_{AB} is denoted as T_{AB}, where $T_{AB}=(t_{ij})$ with $i,j\in\{x,y,z\}$ and $t_{ij}=\mathrm{tr}(\rho_{AB}\sigma_i\otimes\sigma_j)$.

While the star network with $n+1$ parties and n sources shown in Fig. 2 can be considered as an n-independent network. According to Ref. [42], with respect to the generic quantum state $\rho_{A^1A^2}\otimes\rho_{A^1A^3}\otimes\cdots\otimes\rho_{A^1A^{n+1}}$, the maximal value of $\mathcal{B}$ is given by

$$\mathcal{B}_{\mathrm{star}}^{\max}=\sqrt{\prod_{i=1}^{n}(\delta_1^{(i)})^{\frac{2}{n}}+\prod_{i=1}^{n}(\delta_2^{(i)})^{\frac{2}{n}}}. \tag{7}$$

At this time, $\delta_1^{(i)}$ and $\delta_2^{(i)}$ are the two largest eigenvalues of the matrix $\sqrt{T^{\dagger}_{A^1A^{i+1}}T_{A^1A^{i+1}}}$ with $\delta_1^{(i)}>\delta_2^{(i)}$, and $T_{A^1A^{i+1}}$ is the correlation matrix of $\rho_{A^1A^{i+1}}$.

3 The evolution law of quantum states in curved space-time

Note that any two-qubit state can be transformed into a Bell diagonal state through local unitary transformations, without

changing its nonlocality. Therefore, we consider the initial states to be Bell diagonal states, which can be represented as

$$\rho_{AB} = \frac{1}{4}\left(\mathrm{I}_2 \otimes \mathrm{I}_2 + \mathbf{a}\cdot\sigma \otimes \mathrm{I}_2 + \mathrm{I}_2 \otimes \mathbf{b}\cdot\sigma + \sum_i^3 t_i \sigma_i \otimes \sigma_i\right), \tag{8}$$

where $\sigma = (\sigma_1, \sigma_2, \sigma_3), \sigma_i\ (i = 1, 2, 3)$ stand for Pauli matrices. $\mathbf{a}, \mathbf{b} \in \mathbb{R}^3$ denote local bloch vectors. In the following, we will provide the correlation matrices for the physically accessible and inaccessible states after particles interact with Hawking radiation in two cases.

Case 1: Only one subsystem stays at an asymptotically flat region, while the other traverses the event horizon of the black hole.

Using the Kruskal basis shown in Eq. (3) for Alice while keeping Bob stationary, we can reformulate the complete three-partite quantum state $\rho_{A_I A_{II} B}$ associated with the subsystems A_I and B observed by Alice and Bob, respectively, and the subsystem A_{II}, observed by anti-Alice in the interior of a black hole.

Since the interior region of black hole is causally disconnected from the exterior region, Alice and Bob cannot access the modes in the interior region of black hole. By tracing over the inaccessible mode A_{II}, we can obtain the reduced density matrix $\rho_{A_I B}$. We know that in the framework of unitary quantum mechanics, information preservation is obligatory. Although exploring the interior of a black hole is physically impractical, the complete state of our tripartite system is known and maintains unitarity. Consequently, applying a partial tracing operation on the modes A_I within this tripartite state yields the reduced density matrix $\rho_{A_{II} B}$.

Table 1 For the quantum state given by Eq. (8), when Alice freely traverses the event horizon, $T_{A_I B}$ denotes the correlation matrix of the physically accessible quantum state $\rho_{A_I B}$, while $T_{A_{II} B}$ denotes the correlation matrix of the physically inaccessible quantum state $\rho_{A_{II} B}$. Bob's case is similar

Alice freely traverses the event horizon
$T_{A_I B} = \begin{pmatrix} t_1\lambda_- & 0 & 0 \\ 0 & t_2\lambda_- & 0 \\ -b_1\lambda_+^2 & -b_2\lambda_+^2 & t_3\lambda_-^2 - b_3\lambda_+^2 \end{pmatrix}$
$T_{A_{II} B} = \begin{pmatrix} t_1\lambda_+ & 0 & 0 \\ 0 & -t_2\lambda_+ & 0 \\ b_1\lambda_-^2 & b_2\lambda_-^2 & b_3\lambda_-^2 - t_3\lambda_+^2 \end{pmatrix}$
Bob freely traverses the event horizon
$T_{AB_I} = \begin{pmatrix} t_1\lambda_- & 0 & -a_1\lambda_+^2 \\ 0 & t_2\lambda_- & -a_2\lambda_+^2 \\ 0 & 0 & t_3\lambda_-^2 - a_3\lambda_+^2 \end{pmatrix}$
$T_{AB_{II}} = \begin{pmatrix} t_1\lambda_+ & 0 & a_1\lambda_-^2 \\ 0 & -t_2\lambda_+ & a_2\lambda_-^2 \\ 0 & 0 & a_3\lambda_-^2 - t_3\lambda_+^2 \end{pmatrix}$

Table 2 For the quantum state given by Eq. (8), when Alice and Bob freely traverse the event horizon, $T_{A_I B_I}$ denotes the correlation matrix of the physically accessible quantum state $\rho_{A_I B_I}$, while $T_{A_{II} B_{II}}$ denotes the correlation matrix of the physically inaccessible quantum state $\rho_{A_{II} B_{II}}$.

Both Alice and Bob traverse the event horizon
$T_{A_I B_I} = \begin{pmatrix} t_1\lambda_-^2 & 0 & -a_1\lambda_+^2\lambda_- \\ 0 & t_2\lambda_-^2 & -a_2\lambda_+^2\lambda_- \\ -b_1\lambda_+^2\lambda_- & -b_2\lambda_+^2\lambda_- & \lambda_+^4 - (a_3+b_3)\lambda_+^2\lambda_-^2 + t_3\lambda_-^4 \end{pmatrix}$
$T_{A_{II} B_{II}} = \begin{pmatrix} t_1\lambda_+^2 & 0 & a_1\lambda_-^2\lambda_+ \\ 0 & t_2\lambda_+^2 & -a_2\lambda_-^2\lambda_+ \\ b_1\lambda_-^2\lambda_+ & -b_2\lambda_-^2\lambda_+ & \lambda_-^4 - (a_3+b_3)\lambda_+^2\lambda_-^2 + t_3\lambda_+^4 \end{pmatrix}$

Similar operations can be applied to system B, but detailed descriptions are not provided here. Finally, the correlation matrices of the quantum states after different operations are presented in Table 1. The detailed calculation process can be found in the Appendix.

Case 2: Both Alice and Bob traverse the event horizon of the black hole.

Applying the transformation of Eq. (3) to both Alice and Bob, we derive a four-partite state $\rho_{A_I A_{II} B_I B_{II}}$. This state involves modes A_I and B_I observed by Alice and Bob, and modes A_{II} and B_{II} observed by anti-Alice and anti-Bob in the interior of a black hole. Tracing over the inaccessible modes A_{II} and B_{II} gives the reduced density matrix $\rho_{A_I B_I}$. Similarly, tracing over the accessible modes A_I and B_I yields $\rho_{A_{II} B_{II}}$. The correlation matrices for $\rho_{A_I B_I}$ and $\rho_{A_{II} B_{II}}$ are listed in the Table 2.

4 Results and discussion

4.1 Evolution of non-bilocality in the ES network

We start with the ES network characterized by the network state $\rho_{A^1A^2} \otimes \rho_{A^2A^3}$, which corresponds to the simplest forms of the chain network (Fig. 1) and the star network (Fig. 2). We refer to the nonlocal correlations generated by the ES network as nonbilocal correlations or non-bilocality. Considering that the resources $\rho_{A^i A^{i+1}}\ (i = 1, 2)$ distributed on the network is generated from the following family of two-qubit state [43]

$$\begin{aligned}\rho_{A^i A^{i+1}} = {} & v_i|00\rangle\langle 00| + (1 - v_i)[\sin^2 x_1|01\rangle\langle 01| \\ & + \cos^2 x_i|10\rangle\langle 10| + \sin x_i \cos x_i(|01\rangle\langle 10| + |10\rangle\langle 01|)],\end{aligned}$$

where $v_i \in [0, 1]$, and $x_i \in [0, \frac{\pi}{4}]\ (i = 1, 2)$. This class of states has played an important role in demonstrating hidden nonlocality in chain networks [44]. Rewrite it in the Bloch–Fano decomposition yields

$$\begin{aligned}\rho_{A^i A^{i+1}} = {} & \frac{1}{4}\{\mathrm{I}_2 \otimes \mathrm{I}_2 + [v_i - (1 - v_i)\cos 2x_1]\sigma_3 \otimes \mathrm{I}_2 \\ & + [v_i + (1 - v_i)\cos 2x_1]\mathrm{I}_2 \otimes \sigma_3 + (1 - v_i)\sin 2x_1 \sigma_1 \otimes \sigma_1\end{aligned}$$

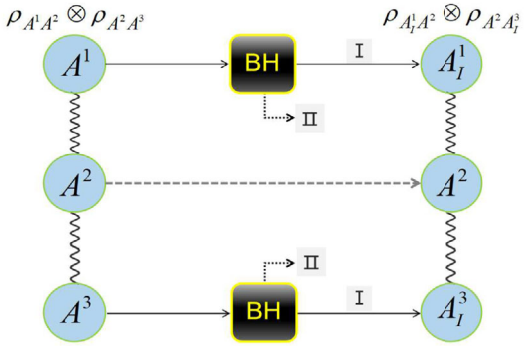

Fig. 3 Schematic diagram of our physical model with particle A^2 in the exterior of a black hole (BH), and particles A^1 and A^3 traversed the event horizon of the BH. The wavy lines show the entanglement between particles. Input state is provided by Eq. (9) and the physically accessible output state has form $\rho_{A_I^1A^2} \otimes \rho_{A^2A_I^3}$

$$+(1-v_i)\sin 2x_1\sigma_2 \otimes \sigma_2 + (2v_i-1)\sigma_3 \otimes \sigma_3\}. \tag{9}$$

Note that the structure of $\rho_{A^iA^{i+1}}$ conforms to Eq. (8).

We will investigate the impact of Hawking radiation on the non-bilocality of $\rho_{A^1A^2} \otimes \rho_{A^2A^3}$ in two scenarios. Scenario 1 is depicted in Fig. 3, where we focus on the changes in A^1 and A^3. Consequently, the final physically accessible network state is $\rho_{A_I^1A^2} \otimes \rho_{A^2A_I^3}$.

According to Table 1 and Eq. (9), we can get the correlation matrices of $\rho_{A_I^1A^2}$ and $\rho_{A^2A_I^3}$ respectively as follows

$$T_{A_I^1A^2} = \begin{pmatrix} t_1^{(1)} & 0 & 0 \\ 0 & t_2^{(1)} & 0 \\ 0 & 0 & t_3^{(1)} \end{pmatrix},$$

where $t_1^{(1)} = t_2^{(1)} = \lambda_-(1-v_1)\sin 2x_1$, $t_3^{(1)} = \lambda_-^2(2v_1 - 1) - \lambda_+^2[v_1 + (1-v_1)\cos 2x_1]$.

$$T_{A^2A_I^3} = \begin{pmatrix} t_1^{(2)} & 0 & 0 \\ 0 & t_2^{(2)} & 0 \\ 0 & 0 & t_3^{(2)} \end{pmatrix},$$

where $t_1^{(2)} = t_2^{(2)} = \lambda_-(1-v_2)\sin 2x_2$, $t_3^{(2)} = \lambda_-^2(2v_2 - 1) - \lambda_+^2[v_2 - (1-v_2)\cos 2x_2]$.

According to Eq. (6) with $n = 2$, the $\mathcal{B}_{\text{biloc}}^{\max}(\rho_{A_I^1A^2} \otimes \rho_{A^2A_I^3})$ depends not only on the state parameters v_i and x_i $(i = 1, 2)$, but also on the Hawking temperature T. Here, we present the calculation results for several specific initial resource states, as shown in Fig. 4.

As illustrated in Fig. 4, $\mathcal{B}_{\text{biloc}}^{\max}(\rho_{A_I^1A^2} \otimes \rho_{A^2A_I^3})$ decreases as the Hawking temperature T rises, indicating that thermal noise from the Hawking temperature induces non-bilocality decay in $\rho_{A^1A^2} \otimes \rho_{A^2A^3}$. The extent of this decay varies case-by-case. When the initial states $\rho_{A^1A^2}$ and $\rho_{A^2A^3}$ are maximally entangled, we have

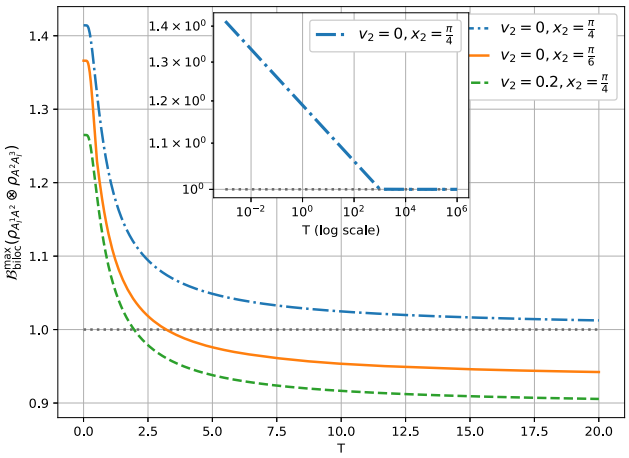

Fig. 4 $\mathcal{B}_{\text{biloc}}^{\max}(\rho_{A_I^1A^2} \otimes \rho_{A^2A_I^3})$ as a function of the Hawking temperature T for the initial $\rho_{A^1A^2}$ being a maximally entangled state (i.e. $v_1 = 0$ and $x_1 = \frac{\pi}{4}$); while $\rho_{A^2A^3}$ is selected from three different states, with their parameters being $v_2 = 0, x_2 = \frac{\pi}{4}$ (maximally entangled state), $v_2 = 0, x_2 = \frac{\pi}{6}$ (entangled pure state), and $v_2 = 0.2, x_2 = \frac{\pi}{4}$ (entangled mixed state). The subfigure illustrates the variation of $\mathcal{B}_{\text{biloc}}^{\max}$ with T on a logarithmic scale when $v_2 = 0, x_2 = \frac{\pi}{4}$

$$\mathcal{B}_{\text{biloc}}^{\max}(\rho_{A_I^1A^2} \otimes \rho_{A^2A_I^3}) = \sqrt{2}\lambda_- = \frac{\sqrt{2}}{\sqrt{e^{-\frac{1}{T}}+1}}. \tag{10}$$

Since $\lim_{T\to\infty} \frac{\sqrt{2}}{\sqrt{e^{-\frac{1}{T}}+1}} = 1$. This implies that even a sufficiently high Hawking temperature will only lead to the weakening of non-bilocality, not its complete disappearance. We have fully demonstrated this phenomenon in the subfigure of Fig. 4 using logarithmic scaling. However, in the other two cases, we observe the "death" of non-bilocality when the Hawking temperature reaches a critical threshold. It is worth noting that the weaker the initial nonlocality, the sooner the "death" occurs. What if the resource states on the network have the same initial non-bilocality?

To reduce the complexity of the calculations, we set $v_1 = v_2 = 0$, in which case $\rho_{A^iA^{i+1}} = |\psi_{A^iA^{i+1}}\rangle\langle\psi_{A^iA^{i+1}}|$, where

$$|\psi_{A^iA^{i+1}}\rangle = \sin x_i|01\rangle + \cos x_i|10\rangle, \quad (i = 1, 2).$$

Then for the initial network state $\rho_{A^1A^2} \otimes \rho_{A^2A^3}$, the maximal value of $\mathcal{B}$ is

$$\mathcal{B}_{\text{biloc}}^{\max}(\rho_{A^1A^2} \otimes \rho_{A^2A^3}) = \sqrt{1 + \sin 2x_1 \sin 2x_2}. \tag{11}$$

In Fig. 5, we present the results of $\mathcal{B}_{\text{biloc}}^{\max}(\rho_{A_I^1A^2} \otimes \rho_{A^2A_I^3})$ for different combinations of $\sin 2x_1$ and $\sin 2x_2$. Note that each set of values ensures that the result of Eq. (11) is $\sqrt{1.64}$.

It can be seen that under the same initial non-bilocality, a larger $\sin 2x_1$ causes $\mathcal{B}_{\text{biloc}}^{\max}(\rho_{A_I^1A^2} \otimes \rho_{A^2A_I^3})$ to decrease more rapidly, indicating faster decay of non-bilocality. Conversely, a larger $\sin 2x_2$ enhances the robustness of non-bilocality

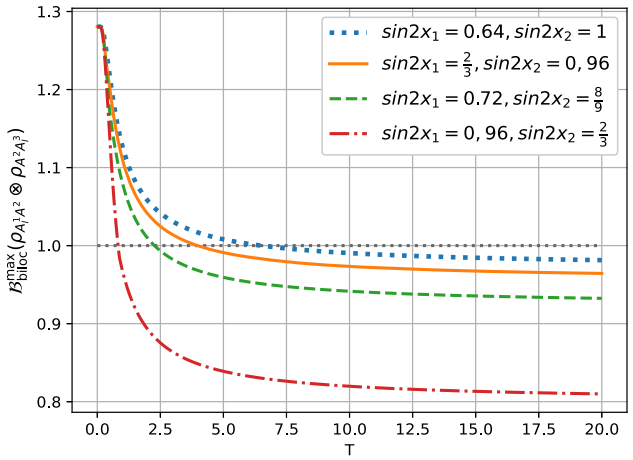

Fig. 5 Let $\rho_{A^i A^{i+1}} = |\psi_{A^i A^{i+1}}\rangle\langle\psi_{A^i A^{i+1}}|$, $(i = 1, 2)$. The quantities $\mathcal{B}^{max}_{biloc}(\rho_{A^1_I A^2} \otimes \rho_{A^2 A^3_I})$ are considered as functions of the Hawking temperature T for four different network states, all of which maintain initial $\mathcal{B}^{max}_{biloc}(\rho_{A^1 A^2} \otimes \rho_{A^2 A^3}) = \sqrt{1.64}$

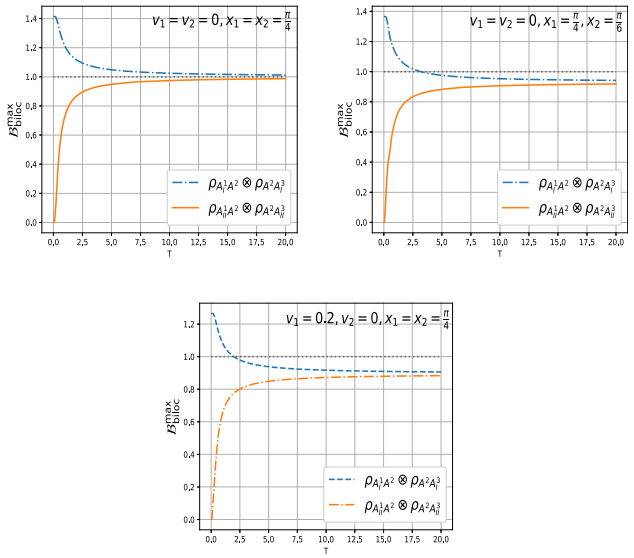

Fig. 6 $\mathcal{B}^{max}_{biloc}(\rho_{A^1_I A^2} \otimes \rho_{A^2 A^3_I})$ and $\mathcal{B}^{max}_{biloc}(\rho_{A^1_{II} A^2} \otimes \rho_{A^2 A^3_{II}})$ as functions of the Hawking temperature T for three initial network states $\rho_{A^1 A^2} \otimes \rho_{A^2 A^3}$

against thermal noise. According to the Horodecki criterion [45], the maximal Clauser–Horne–Shimony–Holt (CHSH) value for $|\psi_{A^i A^{i+1}}\rangle$ $(i = 1, 2)$ is

$$\mathcal{B}^{max}_{CHSH}(\rho_{A^i A^{i+1}}) = 2\sqrt{1 + \sin^2 2x_i}.$$

So, a higher $\sin 2x_i$ corresponds to a stronger quantum nonlocality. Thus, when considering $|\psi_{A^i A^{i+1}}\rangle$ as the resource state, Fig. 5 indicates that if only the marginal particles are affected by the Hawking radiation, assigning quantum states with stronger correlation to $\rho_{A^2 A^3}$ will enhance the robustness of the ES network against the thermal noise generated by Hawking radiation.

In Fig. 3, reducing A^1_I and A^3_I while retaining A^1_{II} and A^3_{II} yields the network state $\rho_{A^1_{II} A^2} \otimes \rho_{A^2 A^3_{II}}$. Due to the causal disconnection between the interior and exterior regions, an observer or detector outside the black hole cannot access information from the interior regions. Thus, the state $\rho_{A^1_{II} A^2} \otimes \rho_{A^2 A^3_{II}}$ is deemed physically inaccessible. Nevertheless, the global quantum state remains unitary and pure. With a prevailing consensus among physicists, including Hawking, favoring the conservation of quantum information, we can theoretically investigate these inaccessible scenarios. To understand where lost quantum correlations reside, we will now examine how Hawking decoherence influences the correlation of network state $\rho_{A^1_{II} A^2} \otimes \rho_{A^2 A^3_{II}}$ in these physically inaccessible contexts.

We still analyze the three network state resources utilized in Fig. 4. Substituting specific parameters from the Table 1 into $T_{A_{II}B}$ and $T_{AB_{II}}$ gives the correlation matrices for $\rho_{A^1_{II} A^2}$ and $\rho_{A^2 A^3_{II}}$, respectively. Figure 6 plots $\mathcal{B}^{max}_{biloc}(\rho_{A^1_{II} A^2} \otimes \rho_{A^2 A^3_{II}})$ as functions of T. It is evident that each example presents similar results. Specifically, in the absence of Hawking decoherence, $\mathcal{B}^{max}_{biloc}(\rho_{A^1_{II} A^2} \otimes \rho_{A^2 A^3_{II}})$ is zero, but as T increases, it gradually increases and eventually stabilizes. Although Hawking radiation enhances its correlation, we have not observed any non-bilocality in any instances. Notably, as the Hawking temperature T increases, both $\mathcal{B}^{max}_{biloc}(\rho_{A^1_I A^2} \otimes \rho_{A^2 A^3_I})$ and $\mathcal{B}^{max}_{biloc}(\rho_{A^1_{II} A^2} \otimes \rho_{A^2 A^3_{II}})$ eventually stabilize at the same value.

In scenario 2, we consider the case where all particles of the network state $\rho_{A^1 A^2} \otimes \rho_{A^2 A^3}$, composed of pure entangled states $|\psi_{A^i A^{i+1}}\rangle$, $(i = 1, 2)$, freely traverse the event horizon. In this case, the physically inaccessible network state can be expressed as $\rho_{A^1_I A^2_I} \otimes \rho_{A^2_I A^3_I}$, and the corresponding correlation matrix can be obtained from $T_{A_I B_I}$ in the Table 2.

According to Fig. 7, we present two key results. First, for $\rho_{A^1 A^2} \otimes \rho_{A^2 A^3}$ composed entirely of maximally entangled states, the blue curve shows that $\mathcal{B}^{max}_{biloc}(\rho_{A^1_I A^2_I} \otimes \rho_{A^2_I A^3_I})$ decreases continuously with increasing Hawking temperature T. Its non-bilocality experiences a "death" at $T = \frac{1}{\ln(\sqrt{2}+1)}$. This is different from the result in Scenario 1. Second, we examine three distinct network states $\rho_{A^1 A^2} \otimes \rho_{A^2 A^3}$ with the same initial value $\mathcal{B}^{max}_{biloc}(\rho_{A^1 A^2} \otimes \rho_{A^2 A^3}) = \sqrt{1.64}$. The three colored curves depict how non-bilocality diminishes for these states as T increases. Although $\mathcal{B}^{max}_{biloc}(\rho_{A^1_I A^2_I} \otimes \rho_{A^2_I A^3_I})$ converges to the same stable value as $T \to \infty$, the subplots show varying initial decay rates among the three states. From this figure, we conclude that when all particles of $\rho_{A^1 A^2} \otimes \rho_{A^2 A^3}$ traverse the event horizon and the pure states $|\psi_{A^i A^{i+1}}\rangle$, $(i = 1, 2)$ are regarded as resource states, assigning stronger quantum correlations to one of the quantum states can enhance the robustness of the ES network against thermal noise.

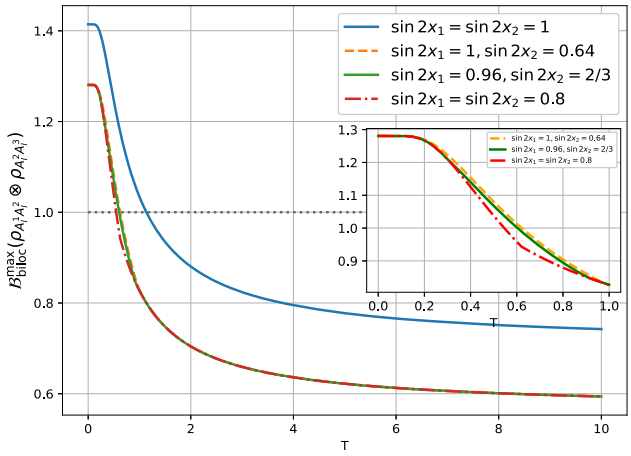

Fig. 7 $\mathcal{B}^{\max}_{\text{biloc}}(\rho_{A_I^1A_I^2} \otimes \rho_{A_I^2A_I^3})$ as a function of the Hawking temperature T. Two specific results are shown, one is initial $\mathcal{B}^{\max}_{\text{biloc}}(\rho_{A^1A^2} \otimes \rho_{A^2A^3}) = \sqrt{2}$ (blue curve), and the other is $\mathcal{B}^{\max}_{\text{biloc}}(\rho_{A^1A^2} \otimes \rho_{A^2A^3}) = \sqrt{1.64}$(orange, green, and red curve). The subfigure demonstrates the trend of the latter case for $T \in (0, 1]$

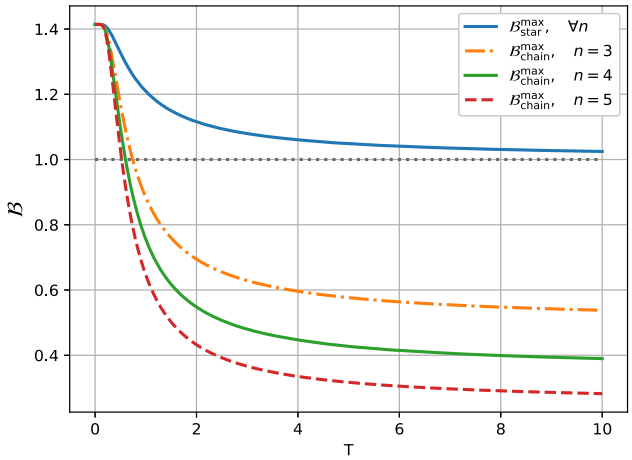

Fig. 8 $\mathcal{B}^{\max}_{\text{chain}}(\rho_{A_I^1A^2} \otimes \rho_{A_I^2A^3} \otimes \cdots \otimes \rho_{A_I^nA^{n+1}})$ and $\mathcal{B}^{\max}_{\text{star}}(\rho_{A^1A_I^2} \otimes \rho_{A^1A_I^3} \otimes \cdots \otimes \rho_{A^1A_I^{n+1}})$ as functions of the Hawking temperature T for different n. Initial $\rho_{A^iA^{i+1}}$ and $\rho_{A^1A^{i+1}}$ $i = 1, 2, \ldots n$ are all maximally entangled states

4.2 Evolution of nonlocality in n-locality scenario

For a general network $\Xi_{q,n}$ consisting of q parties and n sources, which can be regarded as a k-independent network, its non-n-local correlation is detected by violating Ineq. (5). When n resources are fixed, regardless of how they interact with Hawking radiation, the decay of non-n-locality depends not only on the Hawking temperature but also on the number of parties q and the independent number k.

We consider the chain and star network scenarios illustrated in Figs. 1 and 2, respectively. Assume all resource states are maximally entangled states, then based on Eq. (6) and Eq. (7), $\mathcal{B}^{\max}_{\text{chain}} = \mathcal{B}^{\max}_{\text{star}} = \sqrt{2}$. Obviously, both star and chain networks can generate non-n-local correlations now. We will investigate whether the non-n-local correlations of these two networks can persist within the context of a black hole under two scenarios.

In the first scenario, for each bipartite quantum state constituting the quantum network, one subsystem remains in the exterior region of a black hole while the other traverses the black hole's event horizon. For a chain network with sources $\rho_{A^iA^{i+1}}$, we consider the evolution occurring in subsystem A^{i+1} $(i = 1, 2, \ldots, n)$, at this point, the effect of Hawking radiation on its non-n-locality is characterized by

$$\mathcal{B}^{\max}_{\text{chain}}(\rho_{A^1A_I^2} \otimes \rho_{A^2A_I^3} \otimes \cdots \otimes \rho_{A^nA_I^{n+1}}).$$

For a star network with n sources, only subsystem A^{i+1} of $\rho_{A^1A^{i+1}}$ $(i = 1, 2, \ldots, n)$ traverses the black hole's event horizon, while the effect of Hawking radiation on its non-n-locality is characterized by

$$\mathcal{B}^{\max}_{\text{star}}(\rho_{A^1A_I^2} \otimes \rho_{A^1A_I^3} \otimes \cdots \otimes \rho_{A^1A_I^{n+1}}).$$

Given our consideration that all sources are distributed in the maximally entangled state $\frac{1}{\sqrt{2}}(|01\rangle + |10\rangle)$, the maximum Bell inequality violation for the chain network is given by

$$\mathcal{B}^{\max}_{\text{chain}}(\rho_{A_I^1A^2} \otimes \rho_{A_I^2A^3} \otimes \cdots \otimes \rho_{A_I^nA^{n+1}}) = \sqrt{2}\lambda_-^{\frac{2}{n}}$$

and for the star network, it is given by

$$\mathcal{B}^{\max}_{\text{star}}(\rho_{A^1A_I^2} \otimes \rho_{A^1A_I^3} \otimes \cdots \otimes \rho_{A^1A_I^{n+1}}) = \sqrt{2}\lambda_-.$$

In Fig. 8, we show how $\mathcal{B}^{\max}_{\text{chain}}$ and $\mathcal{B}^{\max}_{\text{star}}$ vary with increasing Hawking temperature T. It is noted that for a star network with n resources, $\mathcal{B}^{\max}_{\text{star}} = \sqrt{2}\lambda_-$, which matches the result of Eq. (10). Given that the subfigures in Fig. 4 have already demonstrated $\sqrt{2}\lambda_-$ on a logarithmic scale over a sufficiently large range of Hawking temperatures, we here only present the trends in ordinary coordinates. This result indicates that the non-n-locality of the star network diminishes but does not fully disappear. In contrast, for the chain network, non-n-locality will die out. Notably, as n increases, $\mathcal{B}^{\max}_{\text{chain}}$ decreases more rapidly, leading to an earlier onset of non-n-locality "death".

In the second scenario, the entire network is situated within the black hole horizon and experiences Hawking radiation, the effects of Hawking radiation on non-n-locality of chain network and star network are characterized by

$$\mathcal{B}^{\max}_{\text{chain}}(\rho_{A_I^1A_I^2} \otimes \rho_{A_I^2A_I^3} \otimes \cdots \otimes \rho_{A_I^nA_I^{n+1}}) = \sqrt{2}\lambda_-^{n}$$

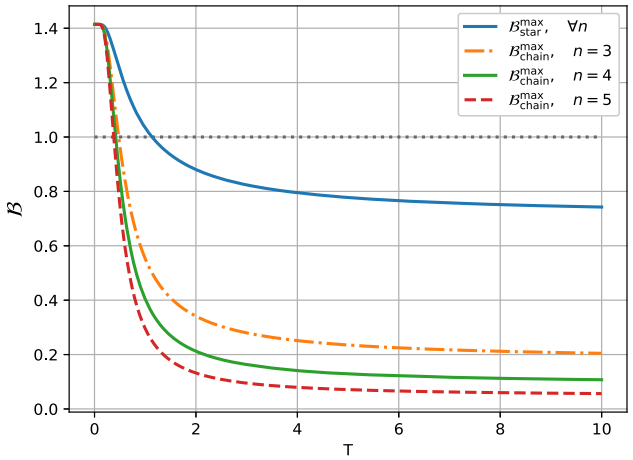

Fig. 9 $\mathcal{B}^{max}_{chain}(\rho_{A^1_I A^2_I} \otimes \rho_{A^2_I A^3_I} \otimes \cdots \otimes \rho_{A^n_I A^{n+1}_I})$ and $\mathcal{B}^{max}_{star}(\rho_{A^1_I A^2_I} \otimes \rho_{A^1_I A^3_I} \otimes \cdots \otimes \rho_{A^1_I A^{n+1}_I})$ as functions of the Hawking temperature T for different n. Initial $\rho_{A^i A^{i+1}}$ and $\rho_{A^1 A^{i+1}}$ $i = 1, 2, \ldots n$ are all maximally entangled states

and

$$\mathcal{B}^{max}_{star}(\rho_{A^1_I A^2_I} \otimes \rho_{A^1_I A^3_I} \otimes \cdots \otimes \rho_{A^1_I A^{n+1}_I}) = \sqrt{2}\lambda_-^2,$$

respectively. In Fig. 9, we present the changing trends of $\mathcal{B}^{max}_{chain}$ and $\mathcal{B}^{max}_{star}$ with the Hawking temperature T. We find that non-n-locality decays more rapidly compared to the first scenario, and the non-n-locality of the star network also undergoes "death" at a certain critical temperature.

Overall, the star network shows more advantages than the chain network in resisting the decay of non-n-locality caused by Hawking radiation. The chain network's sensitivity to thermal noise from Hawking radiation increases with more intermediate nodes.

5 Conclusion

In this study, we characterized the nonlocal correlations of quantum networks within Schwarzschild spacetime. First, we present the variation law governing the quantum state correlation matrix in curved spacetime. Based on this, we analyze changes in non-bilocal correlations under two scenarios, starting with the simplest ES network configuration. It is evident that the Hawking effect degrades non-bilocal correlation, and this degradation is closely related to the initial nonlocality of the network. Furthermore, utilizing a pure entangled state $|\psi_{A^i A^{i+1}}\rangle = \sin x_i|01\rangle + \cos x_i|10\rangle$, $(i = 1, 2)$ as a resource and maintaining constant initial non-bilocal correlation, we discovered that different states and their distribution methods can lead to significantly divergent attenuation trends. Specifically, when only marginal particles are affected by Hawking radiation, maximizing the correlation of right-hand resource states better enhances the resilience of the ES network to Hawking effects. When all particles are subjected to Hawking radiation, it is better to maximize the correlation on one side of the resource state as much as possible. Our research also indicates that it is impossible to establish physically inaccessible non-bilocal correlation.

In larger-scale networks, we observed that even identical states distributed across different network topologies can lead to markedly different variations in nonlocal correlations. We validate this finding in general chain and star networks, with results showing that star networks are more robust against thermal noise from Hawking radiation. Overall, this investigation deepens the understanding of quantum networks operating within curved spacetime.

Acknowledgements This work is supported by the National Natural Science Foundation of China under Grants No.12271394.

Data Availability Statement Data will be made available on reasonable request. [Authors' comment: The datasets generated during and/or analysed during the current study are available from the corresponding author on reasonable request.]

Code Availability Statement Code/software will be made available on reasonable request. [Authors' comment: The code/software generated during and/or analysed during the current study is available from the corresponding author on reasonable request.]

Funded by SCOAP[3].

6 Appendix

First of all, the identity matrix I_2 and the Pauli matrices $\sigma = (\sigma_1, \sigma_2, \sigma_3)$ after interaction with the Hawking radiation Eq. (3) is given by

$$\begin{aligned}
I_{2(I,II)} &= \lambda_-^2|00\rangle\langle 00| + \lambda_-\lambda_+(|00\rangle\langle 11| + |11\rangle\langle 00|) \\
&\quad + \lambda_+^2|11\rangle\langle 11| + |10\rangle\langle 10|, \\
\sigma_{1(I,II)} &= \lambda_-(|00\rangle\langle 10| + |10\rangle\langle 00|) + \lambda_+(|11\rangle\langle 10| + |10\rangle\langle 11|), \\
\sigma_{2(I,II)} &= i(\lambda_-(|10\rangle\langle 00| - |00\rangle\langle 10|) + \lambda_+(|10\rangle\langle 11| - |11\rangle\langle 10|)), \\
\sigma_{3(I,II)} &= \lambda_-^2|00\rangle\langle 00| + \lambda_-\lambda_+(|00\rangle\langle 11| + |11\rangle\langle 00|) \\
&\quad + \lambda_+^2|11\rangle\langle 11| - |10\rangle\langle 10|.
\end{aligned}$$

By tracing over the inaccessible mode $|\cdot\rangle_{II}$, it reduced as

$$\begin{aligned} \mathrm{I}_{2(I)} &= \mathrm{I}_2 - \lambda_+^2\sigma_3, \qquad & \sigma_{1(I)} &= \lambda_-\sigma_1, \\ \sigma_{2(I)} &= \lambda_-\sigma_2, & \sigma_{3(I)} &= \lambda_-^2\sigma_3. \end{aligned} \tag{12}$$

By tracing over the accessible mode $|\cdot\rangle_I$, it reduced as

$$\begin{aligned} \mathrm{I}_{2(II)} &= \mathrm{I}_2 + \lambda_-^2\sigma_3, \qquad & \sigma_{1(II)} &= \lambda_+\sigma_1, \\ \sigma_{2(II)} &= -\lambda_+\sigma_2, & \sigma_{3(II)} &= -\lambda_+^2\sigma_3. \end{aligned} \tag{13}$$

For the quantum state given by Eq. (8), if Hawking radiation only acts on system A, the physically accessible quantum state can be expressed as

$$\begin{aligned} \rho_{A_I B} =& \frac{1}{4}\Big((\mathrm{I}_2 - \lambda_+^2\sigma_3)\otimes \mathrm{I}_2 + \mathbf{a}\cdot(\lambda_-\sigma_1, \lambda_-\sigma_2, \lambda_-^2\sigma_3)\otimes \mathrm{I}_2 \\ &+(\mathrm{I}_2 - \lambda_+^2\sigma_3)\otimes \mathbf{b}\cdot\sigma + t_1\lambda_-\sigma_1\otimes\sigma_1 + t_2\lambda_-\sigma_2\otimes\sigma_2 \\ &+t_3\lambda_-^2\sigma_3\otimes\sigma_3\Big), \end{aligned}$$

where $\mathbf{a}, \mathbf{b} \in \mathbb{R}^3$ represent local bloch vectors. $\mathbf{a} = (a_1, a_2, a_3)$ and $\mathbf{b} = (b_1, b_2, b_3)$. Let $\mathbf{a}' = (a_1\lambda_-, a_2\lambda_-, a_3\lambda_-^2 - \lambda_+^2)$, obviously $|\mathbf{a}'| \leq 1$ due to the range of λ_-, then the reduced state $\rho_{A_I B}$ finally has form

$$\begin{aligned} \rho_{A_I B} =& \frac{1}{4}\big(\mathrm{I}_2\otimes\mathrm{I}_2 + \mathbf{a}'\cdot\sigma\otimes\mathrm{I}_2 + \mathrm{I}_2\otimes\mathbf{b}\cdot\sigma + t_1\lambda_-\sigma_1\otimes\sigma_1 \\ &+t_2\lambda_-\sigma_2\otimes\sigma_2 - b_1\lambda_+^2\sigma_3\otimes\sigma_1 - b_2\lambda_+^2\sigma_3\otimes\sigma_2 \\ &+(t_3\lambda_-^2 - b_3\lambda_+^2)\sigma_3\otimes\sigma_3\big), \end{aligned}$$

and its correlation matrix is

$$T_{A_I B} = \begin{pmatrix} t_1\lambda_- & 0 & 0 \\ 0 & t_2\lambda_- & 0 \\ -b_1\lambda_+^2 & -b_2\lambda_+^2 & t_3\lambda_-^2 - b_3\lambda_+^2 \end{pmatrix}.$$

For the correlation matrix $T_{A_{II}B}$ of $\rho_{A_{II}B}$, simply make the corresponding substitutions using Eq. (13). Similar operations applied to system B can obtain T_{AB_I} and $T_{AB_{II}}$. If both Alice and Bob hover in the interior of a black hole, $T_{A_I B_I}$ and $T_{A_{II}B_{II}}$ can be obtained by transforming the two subsystems of ρ_{AB} simultaneously using Eq. (12) or Eq. (13).

References

1. L. Borgianni, D. Adami, S. Giordano, IEEE Commun. Mag. **62**, 70 (2024)
2. R. Kaltenbaek et al., Exp. Astron. **51**, 1677 (2021)
3. Z. Yuan, J. Zhang, J.W. Pan, Phys. Rev. Lett. **120**, 100501 (2020)
4. J. Zhang et al., IEEE Trans. Aerosp. Electron. Syst. **50**, 931–943 (2020)
5. Zhang et al., Nat. Photon. **13**, 341–346 (2020)
6. K. Schwarzschild, Sitzungsberichte der königlich preussischen Akademie der Wissenschaften. 189 (1916)
7. K. Akiyama et al., Astrophys. J. Lett. **875**(L4), 52 (2019)
8. S.W. Hawking, Nature **248**(5443), 30 (1974)
9. S.W. Hawking, Math. Phys. **43**(3), 199 (1975)
10. S.W. Hawking, Phys. Rev. D **14**, 2460 (1976)
11. S.M. Wu, H.Y. Wu, Y.X. Wang, J. Wang, Phys. Lett. B **865**, 139493 (2025)
12. S.M. Wu, H.S. Zeng, Eur. Phys. J. C **82**, 716 (2022)
13. A. Ali et al., Phys. Rev. D **110**, 064001 (2024)
14. S.M. Wu et al., Phys. Lett. B **848**, 138334 (2024)
15. S.M. Wu et al., Europhys. Lett. **141**, 18001 (2023)
16. J. Shi et al., Phys. A **510**, 649 (2018)
17. W.Y. Sun et al., Laser Phys. Lett. **21**(7), 075202 (2024)
18. Z.Y. Ding et al., Laser Phys. Lett. **14**(12), 125201 (2017)
19. T. Zhang, X. Wang, S.M. Fei, Eur. Phys. J. C **83**, 607 (2023)
20. S.M. Wu, H.S. Zeng, Eur. Phys. J. C **82**, 4 (2022)
21. C. Liu, Z. Long, Q. He, Results Phys. **62**, 107811 (2024)
22. G.W. Mi, X. Huang, S.M. Fei, T. Zhang, Eur. Phys. J. C **85**(3), 1–12 (2025)
23. D. Wang et al., Annalen der Physik **530**, 1800080 (2018)
24. S.M. Wu et al., J. High Energy Phys. **11**, 1–20 (2023)
25. X. Liu, C. Zeng, J. Wang, arXiv:2501.00246 (2025)
26. L.J. Li et al., Eur. Phys. J. C **82**(8), 726 (2022)
27. W. Liu, C. Wen, J. Wang, J. High Energy Phys. **1**, 1–21 (2025)
28. X. Liu, W. Liu, Z. Liu, J. Wang, arXiv:2503.00404 (2024)
29. A. Tavakoli et al., Rep. Prog. Phys. **85**(5), 056001 (2022)
30. M.X. Luo, Phys. Rev. Lett. **120**, 140402 (2018)
31. A. Pozas Kerstjens, N. Gisin, A. Tavakoli, Phys. Rev. Lett. **128**, 010403 (2022)
32. B. Jing et al., Nat. Photon. **13**(3), 210 (2019)
33. W. Ge et al., Phys. Rev. Lett. **121**, 043604 (2018)
34. F. Xu et al., Rev. Mod. Phys. **92**, 025002 (2020)
35. Y.A. Chen et al., Nature (London) **589**, 214 (2021)
36. Z. Zhang, Q. Zhuang, Quantum Sci. Technol. **6**(4), 043001 (2021)
37. J. Jing, Phys. Rev. D **70**, 065004 (2004)
38. T. Damoar, R. Ruffini, Phys. Rev. D **14**, 332 (1976)
39. A. Fabbri, J. Navarro Salas, Modeling black hole evaporation. (2005)
40. R. Kerner, R.B. Mann, Phys. Rev. D **73**, 104010 (2006)
41. A. Kundu et al., Phys. Rev. A **102**(5), 052222 (2020)
42. F. Andreoli et al., New J. Phys. **19**(11), 113020 (2017)
43. W. Kłobus et al., Phys. Rev. A **86**(2), 020302 (2012)
44. K. Mukherjee et al., Phys. Rev. A **108**(3), 032416 (2023)
45. R. Horodecki, Phys. Lett. A **200**(5), 340 (1995)